Bachelor's project
Material science and engineering

Atomistic simulation of cementitious system

Charge distribution in the C-S-H interlayer

BONVIN Jérémie
Student, Material science and engineering, EPFL

Supervisors

ČASAR Žiga, BOWEN Paul
Laboratory of construction materials LMC, IMX, EPFL

Abstract

This work provides a method to analyze the charge distribution in the CSH interlayer. It starts with a qualitative overview based on contour plots. Then it provides many quantitative analyses based on: a point pattern description, a dispersion index and a analysis of polyhedrons. The results are compared with the energy stability of the structure. The main points of the discussion present further investigations that should be performed to ensure the validity of the results. The results do not show clear trends between the energy stability of the structure and the charge distribution. It can be argued that many charge compensation mechanisms exist and have a similar energy stability.

Table of contents

Chapter 1

Introduction

During the last century, residential areas have grown in size and in density. Cement has been the conventional construction material during this huge development. Indeed, due to its remarkable characteristics, durability, and low cost, it has become the most widely used material on the planet [1]. Behind these benefits, the environmental footprint is becoming increasingly problematic. The concrete industry is thus conducting extensive research to reduce its carbon impact.

The main issues to be addressed to reduce the carbon footprint of the concrete industry are the optimisation of clinker production and the reduction of its use. It is estimated that it will account for 5–8% of global emissions [2]. Furthermore, there are additional concerns, such as the availability of certain cement components. It is therefore necessary to develop alternatives to ensure the long-term viability of the concrete industry. The United Nations report on environmentally friendly cement [1] offers solutions. The two primary methods presented are the use of alternative clinkers and the use of substitute materials known as supplementary cementitious materials (SCMs). These solutions incorporate the difficulties of understanding the relationships between macroscopic characteristics and microstructure. Such insights enable not only better formulations of cement, but also reduce the use of clinkers (high CO_2 cost) for materials with a low CO_2 cost without compromising the so-appreciated qualities of concrete.

The cement community is focused on improving the understanding of cement chemistry and hydration kinetics in order to allow better formulations of cement. The current project follows this trend. The project consists of analyzing the charge distribution in the C-S-H interlayer using atomic scale modeling and molecular dynamics. This is important regarding the hypothesis that the charge of the bulk plays a role in the adsorption phenomena and so in the hydration process.

Chapter 2

State of the art

2.1 Portland cement

Portland cement (PC) is the most commonly used cement formulation. Its composition is fairly well known. The PC divides itself into a large variety of classes, which are defined according to their composition. Despite this variety, the primary phases of PC are Alite (impure tricalcium silicate) and Belite (impure dicalcium silicate), which account for more than 70% of the cement weight [3].
Hydration of Alite is the main process that governs the peak of hydration of cement. This period is important for determining the early age mechanical properties of the material. Calcium silicate hydrate (C-S-H) is the main hydration product during this peak. The nucleation and growth of this phase are critical for understanding the hydration mechanism.

2.2 Early work on C-S-H

Early investigations of C-S-H have shown its nanocrystalline nature. It has also been shown to be comparable to the natural minerals Tobermorite and Jennite [4]. However C-S-H phases have various Ca:Si composition ratios [5] against a constant and much lower ratio for these minerals. Later, some models involving the mixing of phases have been presented. However, research on this phase has intensified in the last 20 years, culminating in the publication of novel methods to characterize the C-S-H and more accurate models to describe it.

2.3 C-S-H Bulk structure model

Abhishek Kumar et al. [6] have published a new approach for synthesizing C-S-H with a homogeneous and controlled Ca:Si ratio. Further analysis of samples prepared with this method confirms the crystallographic model of defective Tobermorite 14Å. In contrast to previous models, this completes the description of C-S-H without requiring the inclusion of a second phase.

Simultaneously, Aslam Kunhi Mohamed et al. [7] created a new approach termed the "building brick model," which is specifically designed to form C-S-H structures and incorporate defects in them. Because the stoichiometry of C-S-H varies within it, this model is essential for modeling the phase of C-S-H in cementitious systems. Other investigations have revealed the difference in the composition of the C-S-H interlayer compared to Tobermorite [8]. Most of the cementitious material community agrees on the previously outlined models.

2.4 C-S-H Surface model

Unlike the bulk structure, the surface structure of C-S-H is poorly known. Although the specific surface area of this phase has been demonstrated to be around $200 - 300 m^2/g$, it varies depending on

the drying procedure or the degree of hydration. The unpublished article of Ziga Casar et al. [9] shows that the use of two interlayer thick sheets of C-S-H model is consistent with experimental results. Then the paper explores different surface terminations for a bulk structure of Ca/Si ratio of 1.7. The results suggest that the model of mixed, silicate and calcium terminated, surfaces is the best to describe the surface charges.

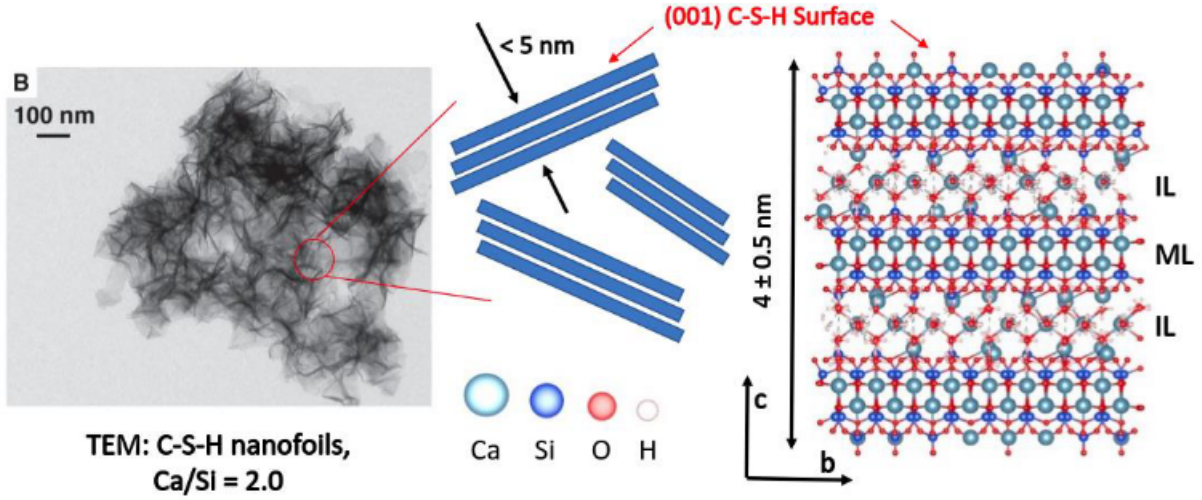

Figure 2.1: C-S-H nanofoils. Measured thickness of approximately 3.5nm matches the C-S-H model structure with two interlayers. TEM from Kumar et al. [6]. IL – interlayer, ML – main layer [9]

Current research is focused on the development of new practical methods to characterize surfaces. These methods test the surface models that are developed simultaneously. Correctly representing surfaces is essential since it is already known that the surface termination influences the orientation of the water at and close to the surface, which impacts features such as hydrodynamic behavior. This has been demonstrated for the Tobermorite structure by Andrey G.Kalinichev et al. [10].

2.5 Atomic scale modeling

Atomic-scale modelling is now used in almost every branch of research. During the last few decades, there has been an increase in the use of atomic-scale modeling in cementitious research. The study performed by Mohammad Javad Abdolhosseini Qomi et al. [11] exemplifies the significance of such an approach in research. Indeed, deeper understanding of adsorption phenomena in cementitious systems allows the scientific community to explore new ways to reduce the shrinkage of cement pastes. As well-stated by Nicolas Marzari [12] the goal of atomic-scale modeling in material science is either to model structures that are coherent with experimental data or to improve the coherence of the analytical results and the modeling results. As Aslam Kunhi Mohamed et al. point out in a recent review paper of molecular modeling of cementitious admixtures [13], molecular modeling must be carefully used to answer pressing questions and to obtain important results to reduce the carbon footprint of the concrete industry.

2.5.1 The block model & the brick code

As already stated, Aslam Kunhi Mohamed et al. have recently provided a new approach to construct the atomic structures of C-S-H and to verify the models with experimental results. This approach encodes a C-S-H structure as a simple readable string of characters. Small units were built in order to implement defects in wanted areas. These smaller units are named *building blocks* and some are introduced in Table 2.1.

Table 2.1: Descriptions of the main block used by the brick code

Block	Composition
<L	$CaSiO_4$
<Lo	$CaSiO_3OH$
>L	$CaSiO_3$
>Lo	$CaSiO_2OH$
<R	$CaSiO_2$
<Ro	$CaSiO_2OH$
>R	$CaSiO_4$
>Ro	$CaSiO_3OH$

The recently developed *pyCSH* code [14] which builds randomly C-S-H structures, is an automated procedure that generates C-S-H bulk structures that correspond to the experimentally obtained values of mean chain length, Ca/Si ratio, percentage of silanol groups, etc. Essentially, it takes all potential configurations of the upper and lower chains and combines them with the use of Gaussian functions to produce C-S-H structures with desired characteristics. The brick code constructs the structure file cell by cell in the c-direction (it constructs as many layers as wanted), then in the b-direction, and finally it expands the same procedure in the a-direction. The atom's positions are designed for LAMMPS, meaning that the 0th cell is at the origin of the system. The pyCSH brick code builds the cells as follows:

- Construction of the upper left block
- Filling the bridging site
- Construction of the upper right block
- Filling interlayer components
- Same construction for the bellow chain
- Add water in the structure

Chapter 3

Methodology

3.1 Material

In this work, the structure studied is a C-S-H structure with a Ca/Si ratio of 1.7, build with the pyCSH brick code [14]. The simulations are carried out using the MD program LAMMPS [15]. The force field used is the ERICAFF2, which was recently published by M. Valavi et al. [16]. The work performed and the files used are available on Github [17].

3.2 Simulation performed

Different but almost identical simulations have been performed. The first time follows the below description (left) and is used to perform the qualitative analysis. The second type of simulation is used to compare different types of hard minimization in order to then compare them regarding to the charge distribution of the interlayer and their energy stability. They follow the following path (right):

- O-H equilibration
- Core shell equilibration
- Hard minimisation consisting of
  - 200 ps NVT at 300K
  - 200 ps NVT at 1000K
  - 100 ps NVT at 300K
  - 100 ps NVT at 1000K
- Equilibration mw
  - 200 ps NPT at 300K and 1 bar
- Production mw
  - 300 ps NPT at 300K

- O-H equilibration
- Core shell equilibration
- Hard minimisation consisting of cycles
  - 200 ps NVT at 300K
  - 200 ps NVT at 1000K
- 200 ps NVT at 300K
- Equilibration mw
  - 3 ns NPT at 300K and 1 bar
- Production mw
  - 1 ns NPT at 300K

For the quantitative analysis, the simulations are named after the number of cycles performed.

3.3 Data treatment

3.3.1 Goal

The goal of the post-treatment was to identify the charge distribution in the interlayer. To perform such an analysis, it is first necessary to divide the structure into unit cells. The interlayer definition is also an issue.

3.3.2 Point Locations

The structure of each unit cell is defined with the *building brick code* which randomly chooses the introduced defect (occupancy of the bridging site, interlayer and water content). While each unit cell of the supercell is randomly chooses to replicate the experimental values (Ca/Si, MCL, Si-Oh/Si), the data file is still build in a systematic order as mentioned beforehand. This systematic order enables to identify the oxygen atoms of interest, which are on the boundary between different unit cells and therefore represents the coordinates for unit cell separation inside the supercell system. This periodicity is shown in Figure 3.1.

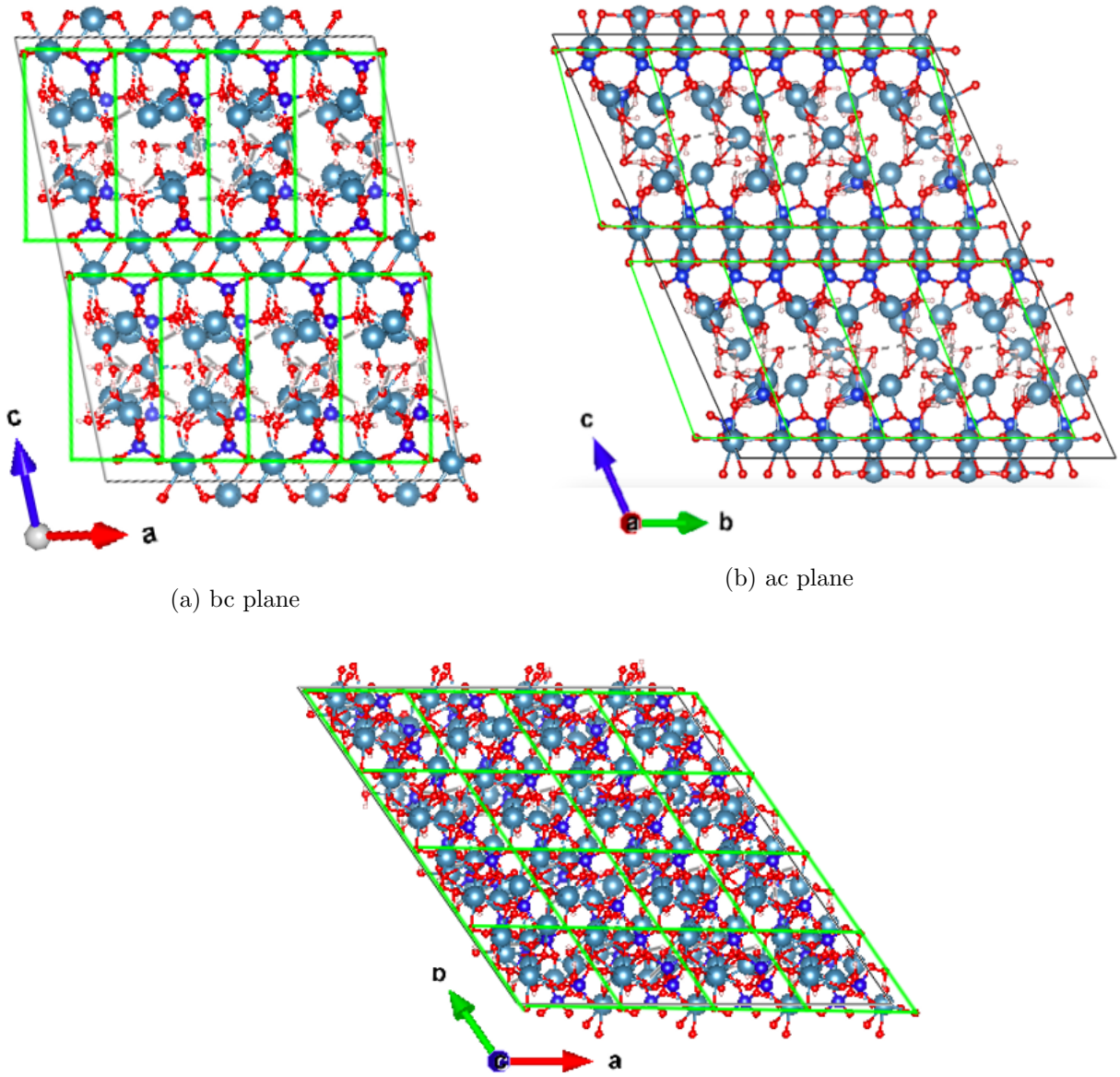

(a) bc plane

(b) ac plane

(c) ab plane

Figure 3.1: Definition of the unit cells: C-S-H 1.7 like Tobermorite 14 $\mathring{A}$ build with the pyCSH code

The oxygen is shared between atoms groups of two different chains, so their coordinates can be used to divide the supercell into separate unit cells. The Figure 3.2 shows that the two atoms that repeat periodically are the 5th atom of the upper layer right block $< r$ and the 5th atom of the lower layer right block $> r$.

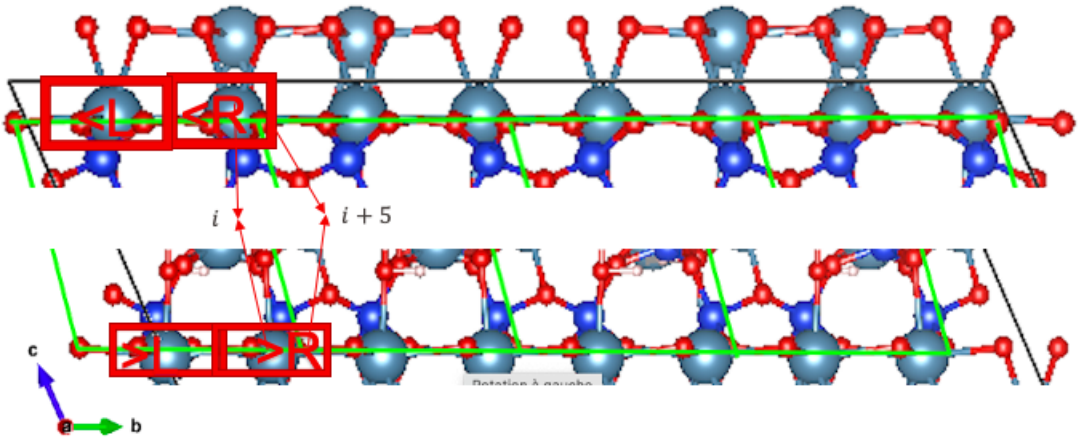

Figure 3.2: Recoginition of the O atoms that define the cells in the structure file thanks to the brick code

It is also needed to take into account the periodic boundary conditions of the supercell system, which is straightforward. When looking along the same silicate chain in can be seen that the unit cells positioned at b_{min} and b_{max} share the same oxygens. Because of this, as illustrated in Figure 3.3, no complicated implementation of periodic boundary conditions needs to be considered, and the shared oxygens can be chosen strictly by the geometry of the system.

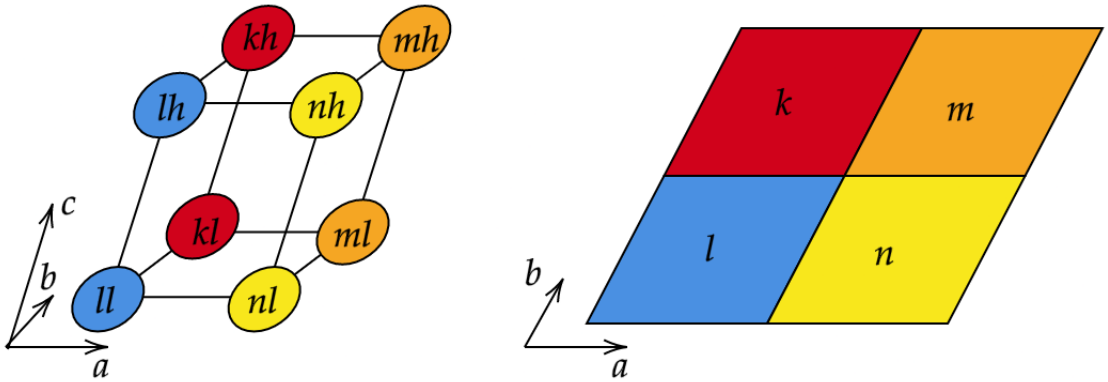

Figure 3.3: Points used to define the kth cell of the structure

This defines the cells through the simulation and so it analyzes the evolution of the charge distributions. Because throughout the simulations the chains would not change, it is possible to locate points defining the cells throughout the simulation.
Once the unit cells are defined, the coordinates of these shared oxygens are used to define planes. Based on the normal of the plane, one can identify if a certain point (in this case, the interlayer species) is located inside or outside of the unit cell. If $f(x, y, z) = 0$, the function f presented below is equivalent to the plane equation.

$$f(x, y, z) = ax + by + cz + d \tag{3.1}$$

While inserting any point (x, y, z) in the function above, it is possible to conclude on which side the point lies given the normal $[a, b, c]$ direction. Obviously, if the function is equal to zero, it means that the point lies in the plane.
During this step, the inside normals are defined by computing the following cross product:

$$\mathbf{n} = (\mathbf{Ol2} - \mathbf{Ol1}) \times (\mathbf{Oh} - \mathbf{Ol1}) \tag{3.2}$$

With $\mathbf{Oh} = (\mathbf{Oh1} + \mathbf{Oh2})/2$ being the average of the point of the upper chain. The Figure 3.4 shows the geometry use for these computations.

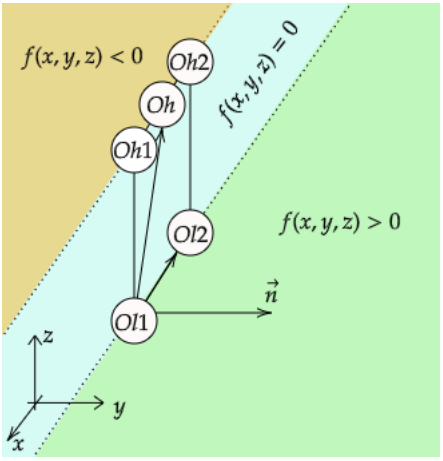

Figure 3.4: Definition of the normal of the plane ; the plane in blue & two half space defined by the plane (orange and green)

If the operation is repeated on all planes of a cell, it can be concluded if a point is inside or outside. That method comes from basic geometry rules [18]. Such analysis allows the division of the structures in many cells. Because the analysis described below has precise needs, the division has only been done in the a direction and in the z-direction, where a simple if condition is enough to divide the cell into two layers in the z-direction. Four rows have been cut in the a-direction. These divisions are shown in the Figure 4.1.

3.3.3 Qualitative overview

With such a division of the structure, it is possible to have a glance at the repartition of charges by computing a contour plot. These plots are computed using the Matplotlib library [19]. It is made with a grided space based on linear interpolations. Other methods, such as Kernel density estimation [20] could be used, but the linear interpolation is considered enough for the previous needs. A typical contour plot consists of the projection of a 3D space on a plane, like geographic maps. A contour plot is displayed in Figure 3.5.

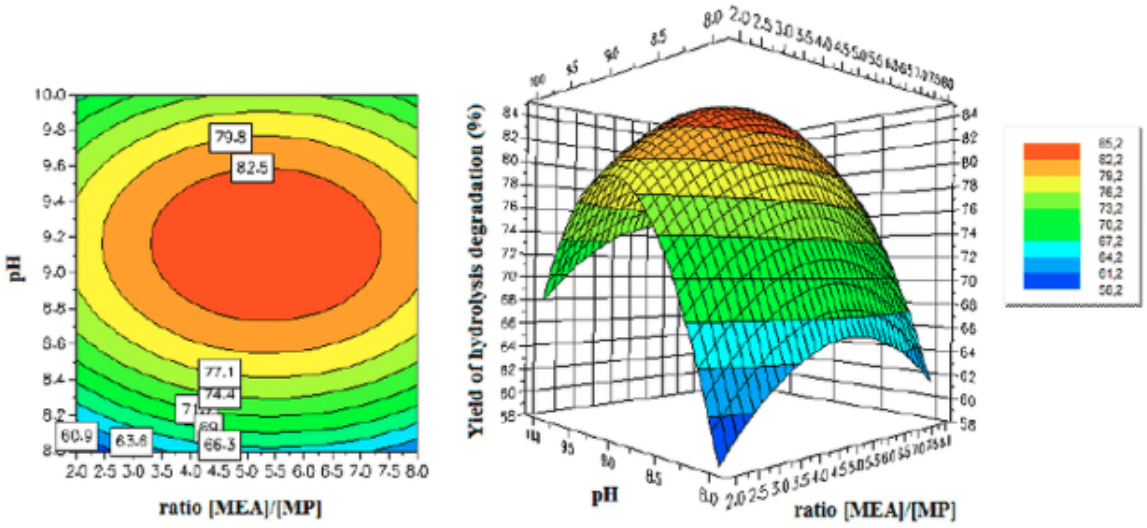

Figure 3.5: Contour plot of a 3D space (here perfomed with MATLAB) [21]

3.3.4 Quantitative overview

Nearest neighbors average distance (NNA)

In order to compute a quantitative analysis of the charge distribution, the first step is to characterize the point pattern through the interlayer. The method of the nearest neighbors average provides a method for recognising structures that are clustered, randomly distributed or periodically distributed (such as in a perfect crystal). This is well shown by M. Gimond [22]. Examples are shown in Figure 3.6.

(a) Single cluster pattern (b) Two clusters pattern (c) Random distribution pattern

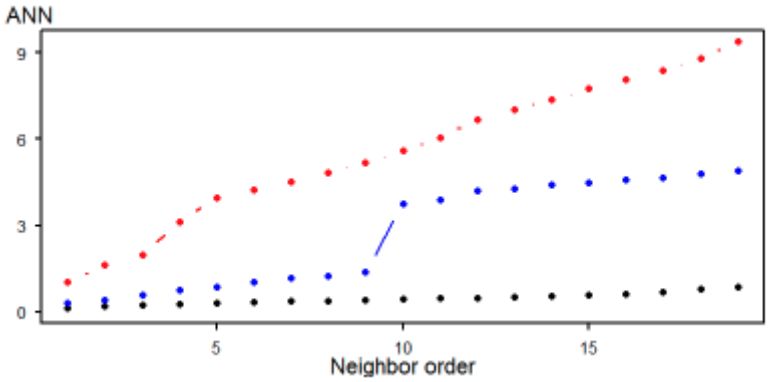

Figure 3.6: Nearest neighbors average method to recognize the point pattern: (a) black, (b) blue, (c) red [22]

Dispersion index γ

The previous analysis (NNA) does not consider the nature of the point. A dispersion index has been defined in order to get further information and be able to perform a comparison between the charge distribution and the energy stability. This index is inspired by the work of Weltens et al. that analyzes the homogeneity of the speed of gas in a catalytic converter [23]. The dispersion index, rho_t, is calculated as shown below:

$$\rho_{t_i} = \frac{1}{n} \sum_{k}^{n} \frac{q_k}{d_{ik}} \tag{3.3}$$

With q_k the charges of the atoms k and d_ik the distance between the ith and the kth atoms. ρ_{t_i} represent the mean charge neighbouring a point i with a factor $(\frac{1}{d_ik})$that decrease its relative contribution while the distance to the point i increase. The mean is made on n neighbors. The choice of n is made regarding the structure.

$$\bar{\rho_t} = \frac{1}{N} \sum_{i}^{N} \rho_{t_i} \tag{3.4}$$

With $\bar{\rho_t}$ representing the mean of ρ_{t_i} through a given structure composed of N atoms.

$$\gamma = \frac{\rho_t}{\rho_0} \tag{3.5}$$

The γ index compares the charges dispersion index through the time.

One of the interests of this formulation is that it is possible to focus on precise type of bonds. With further investigation it is per example possible to compute the evolution of $Ca - Oh$ distances and further analysis.

Calcium polyhedron coordination analysis

The computation of the calcium polyhedron bond type and density has been done with the help of the VESTA visualiser that automatically allows to get such information. Then it has been needed to manually click on each polyhedron in order to print out their bond information. Then a program that analyse the *.txt* files allowing to combine all information together is compiled. The number of $Ca - Oh$ bonds contained in polyhedrons and the density of bonds in polyhedrons are computed.

Energy stability of the structure

In order to compile the energy stability of the structure, its enthalpy is analyzed as a function of times. Given that there are fluctuations due to use of MD, the moving average of the enthalpy is computed to visualize the results. The moving average parameters are: an average window of 100 data points.

Chapter 4

Results

As well shown by a scatter plot in three dimensions, the program divide the space into multiple area, it is shown in Figure 4.1.

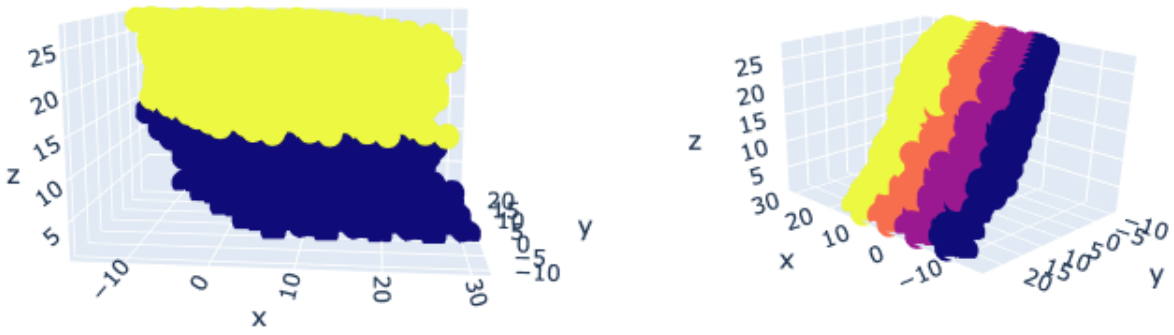

(a) ab slices

(b) bc rows

Figure 4.1: Division of the structur in ab slices (a) corresponding to one interlayer or in bc rows (b) ; unit [Å]

4.1 Qualitative overview

The qualitative overview consists, as mentioned in the previous chapter, of an overview of the charge distribution with contour plots. The Figure 4.2 & 4.3 shows the contour plots of a bc row and of an ab plane.

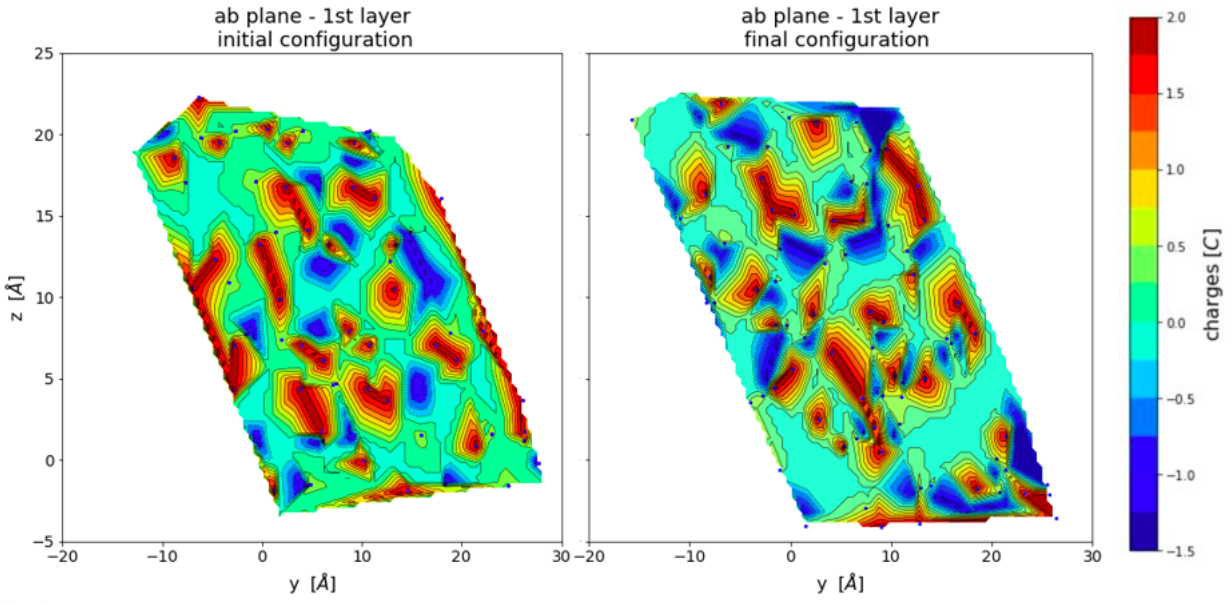

Figure 4.2: Contour plot of bc planes of the 3rd row of cells in the a-direction

It is noticeable that positive +2 charges, i.e. Calcium ions, agglomerate in small clusters.

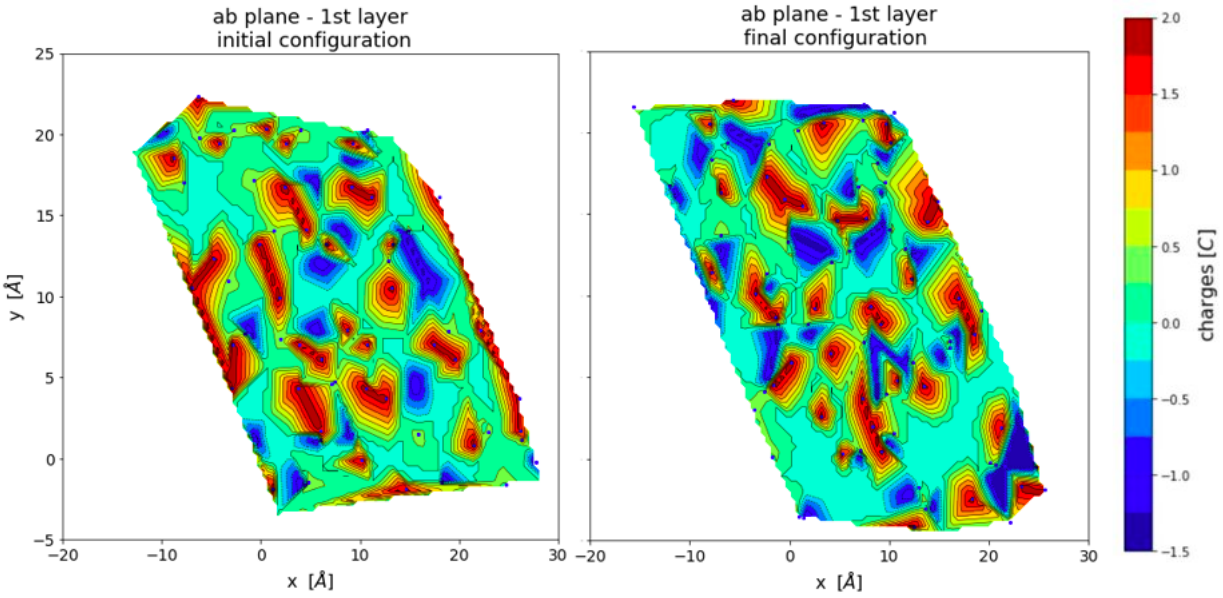

Figure 4.3: Contour plot of ab planes of the 1st interlayer in the c-direction

It is also noticeable that through the simulations, the Ca^{2+} ions move through the interlayer, probably in order to reach local minima of energy.

4.2 Quantitative Overview

4.2.1 Nearest Neighbors Average (ANN) distance

The nearest neighors average distance plots show a huge increase through the first five neighbors, and then it takes the trend of a regular increase. It is clear that there is little clusters of less than five atoms. While comparing different structures, it is evident that the distance decreases through a simulation (Figure 4.4). It is also noticeable that the non-minimization simulation shows a higher ANN distance than the simulations that undergo cycles of hard minization (Figure 4.5). The three other simulations show a similar ANN distance.

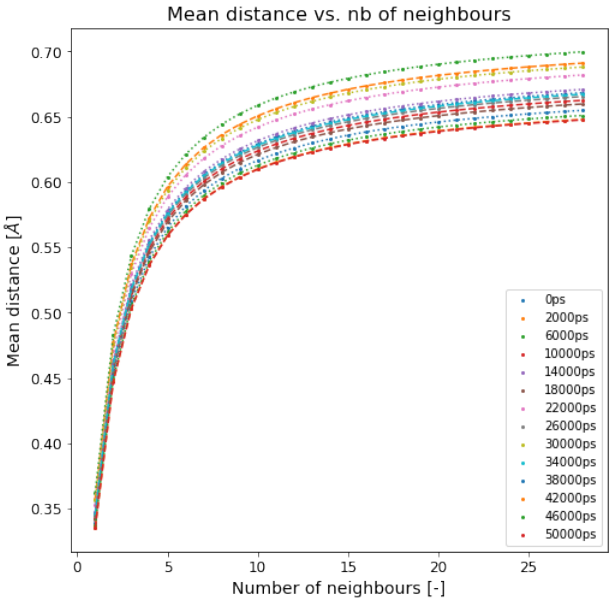

Figure 4.4: NNA distance of 2 cycles simulation through time

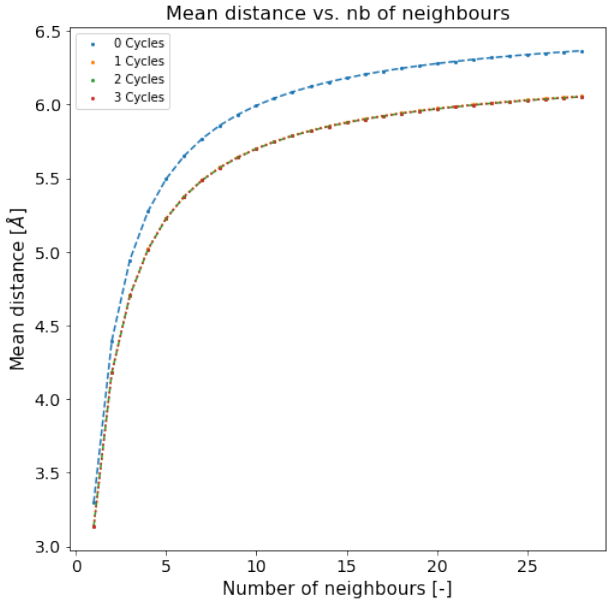

Figure 4.5: NNA distance of last time step of different simulations

Due to these results, the dispersion index will be computed with only four neighbors.

4.2.2 The dispersion index - γ

As defined the γ index shows relatively to an initial configuration if a structure shrinks or expands. It is noticeable that the one cycle hard minimization behaves completely differently than other simulations if computed on the whole interlayer. The Figure 4.6 shows that the one cycle simulation undergoes a slight expansion and the other ones a slight shrinkage which confirms previous statement. While considering only the $Ca - Oh$ distances, which mostly contribute to the local charge neutrality in the interlayer, it is noticeable that all simulations behave similarly, but the 1 cycle simulation undergoes a weaker shrinkage than the others.

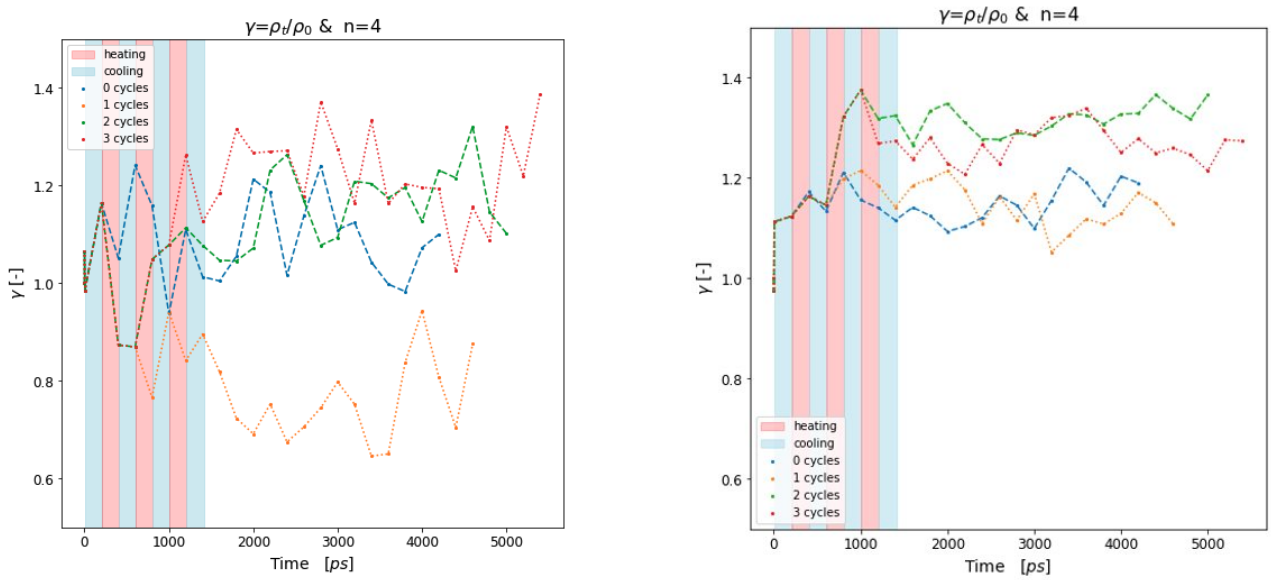

(a) All distances

(b) $Ca - Oh$ distances

Figure 4.6: Analysis of the dispersion index, γ is plot as a function of time

4.2.3 Calcium polyhedron coordination

While carrying out the polyhedron analysis, it is noticeable that there is a clear difference between the one cycle minimization and others (Figure 4.7). As shown by Figure 4.7 (a) & (b), the one cycle simulation has a lower number of bonds than other ones and also a lower density of bonds per polyhedron.

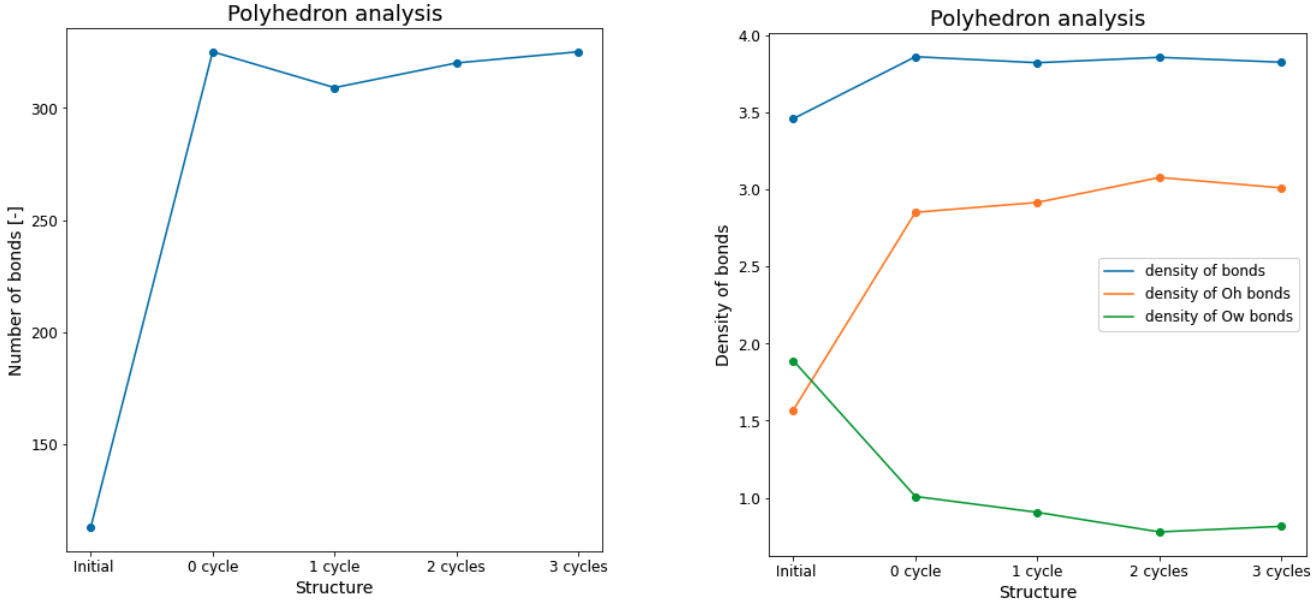

(a) Number of Ca-Oh bond

(b) Density of bonds per polyhedrons

Figure 4.7: Polyhedron analysis results

4.2.4 Energy stability of the structure

While looking at the energy stability of the structure shown in Figure 4.8, it is remarkable that the one cycle hard minimization is enough to reach a local minimum of energy. Further hard minimization does not significantly influence the energy of the structure. It is slightly notable that further minimization increases the enthalpy of the structure.

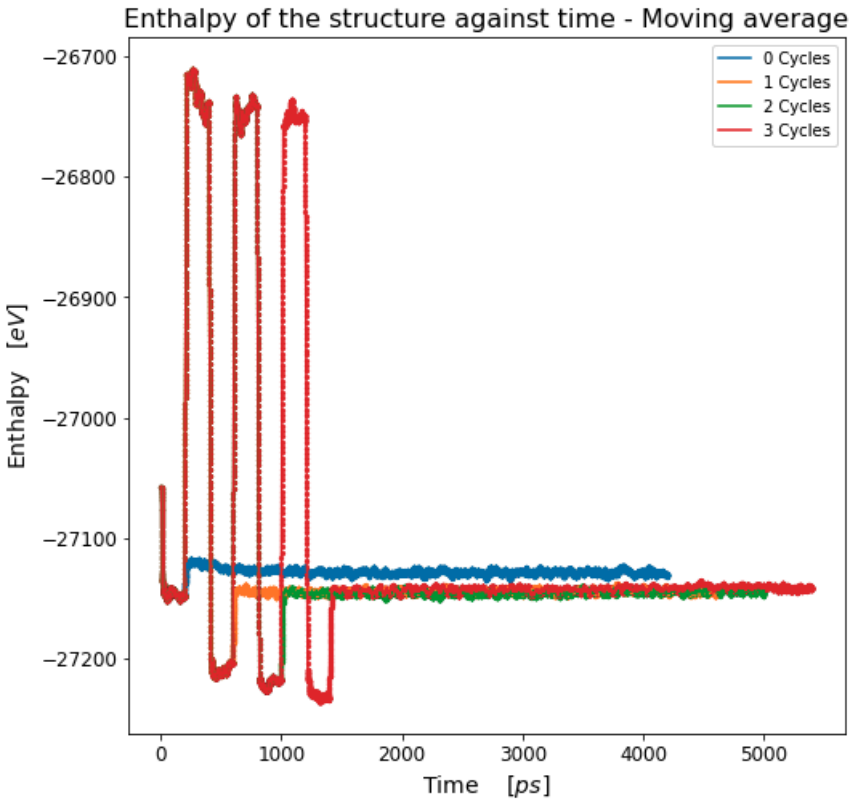

Figure 4.8: Enthalpy of the structure through simulations

Chapter 5

Discussions

Firstly, conclusions cannot be drawn from the contour plot study. Indeed, as information in one dimension is lost, it is not reliable to draw any conclusions. The preliminary conclusions shown in the results chapter are only hypotheses, not facts.
The NNA distance study shows that the atoms are shrinking relatively to each other during a simulation and that the NNA distance does not evolve across different types of hard minimization (Figures 4.4 & 4.5) . This is noticeable because the 1 cycle hard minimization achieves the same order of magnitude of NNA distance as the many cycle hard minimization. Nothing about their differences can be concluded from this plot. However, the dispersion index provides additional informations, clearly demonstrating that the one cycle hard minimization acts differently than the other ones (Figure 4.6). In contrast to earlier simulations where the charges shrink, the charges expand relatively to other atoms. But while analyzing the dispersion index of $Ca - Oh$ distances, it also claims that the one cycle simulation reacts differently. As shown, the shrinkage of $Ca - Oh$ distances is less significant than in other simulations.
All these observations argue that the local minima of energy reached by different types of hard minimzation do not have the same charge distributions. Further examinations and controls on the structure should be done to confirm such a judgment.

To go further, criticism and improvements

To advance, the approach must be improved significantly. To begin, different definitions of the interlayer must be used to understand the mechanisms of charge compensation that contribute to the interlayer's stability. Indeed as the interlayer is not isolated it definition could vary and the results also. Per example including the bridging sites to the study could provides further information about the charge distribution. A such extension of the study helps to understand the charge distribution and the underlying mechanisms. With the same aim, other pair of atoms distances needs to be analyzed apart ($Ca - Ca$, ...). The development of an homogeneity index that is similar to the dispersion index but takes out the homogeneity of the dispersion through the interlayer might also aid in the completion of such an investigation.
Finally, it is evident that the literature with regard to the computation of polyhedron comes mostly from crystal description. According to Pauling's work on crystalline structure prediction given the nature of anions and cations: more the polyhedrons share their content, less stable the structure is [24]. Because the content of the interlayer is not a perfect crystalline structure other Pauling rules cannot be applied, but the 3rd rule associate the crystallographic arrangement of a structure with its stability. Such an analysis might be readily accomplished by determining the density of anions per polyhedron and combining these with the geometry of the polyhedrons. Given these information, it possible to conclude how many anions (i.e. corners) are shared. It is also a way to distinguish the stability of the interlayer. Then, by comparing the same data for different hard minimizations, it should be possible to determine why the enthalpy of the one cycle hard minimization is slightly lower than other ones. Because this work does not deal with single crystals but with a nanocrystalline structure, the approach provided should be investigated further to confirm its reliability.

Chapter 6

Conclusion

The results do not show a clear relationship between the energy stability and the charge dispersion. Indeed, no relations between the overall trend of dispersion index and the energy stability was found. However, it is straightforward that one cycle of hard minimization is enough to reach a local minima of enthalpy, despite it shows a lot of difference with other hard minimization. These findings are quite intriguing, and additional research is needed to understand the causes and variations across the hard minimizations.
Because the work has only been performed on a CSH structure with a Ca/Si ratio of 1.7 , it is noticeable that methods should be verified on well known structures such as the tobermorites. It will allow then to apply the same procedure to more complex atomic structures.

Acknowledgment

First of all, I would like to thank Žiga Časar for the pleasant working environment he offered and all the support he offered. Then, I would like to thank professor Paul Bowen and professor Karen Scrivener for giving me the opportunity to work for the Laboratory of construction material (LMC) with this project. Finally, I want to thank my colleague Tecla Bottinelli Montandon for the support and the help on monday morning.

Bibliography

[1] K. L. Scrivener, V. M. John, and E. M. Gartner, "Eco-efficient cements: Potential economically viable solutions for a low-CO2 cement-based materials industry," en, *Cement and Concrete Research*, Report of UNEP SBCI working group on Low-CO2 eco-efficient cement-basedmaterials, vol. 114, pp. 2–26, Dec. 2018, ISSN: 0008-8846. DOI: 10.1016/j.cemconres.2018.03.015. [Online]. Available: https://www.sciencedirect.com/science/article/pii/S0008884618301480 (visited on 04/11/2022).

[2] K. L. Scrivener and R. J. Kirkpatrick, "Innovation in use and research on cementitious material," en, *Cement and Concrete Research*, Special Issue — The 12th International Congress on the Chemistry of Cement. Montreal, Canada, July 8-13 2007, vol. 38, no. 2, pp. 128–136, Feb. 2008, ISSN: 0008-8846. DOI: 10.1016/j.cemconres.2007.09.025. [Online]. Available: https://www.sciencedirect.com/science/article/pii/S0008884607002347 (visited on 04/11/2022).

[3] *Portland cement*, en, Page Version ID: 1080045371, Mar. 2022. [Online]. Available: https://en.wikipedia.org/w/index.php?title=Portland_cement&oldid=1080045371 (visited on 04/11/2022).

[4] I. G. Richardson, "Tobermorite/jennite- and tobermorite/calcium hydroxide-based models for the structure of C-S-H: Applicability to hardened pastes of tricalcium silicate, -dicalcium silicate, Portland cement, and blends of Portland cement with blast-furnace slag, metakaolin, or silica fume," en, *Cement and Concrete Research*, H. F. W. Taylor Commemorative Issue, vol. 34, no. 9, pp. 1733–1777, Sep. 2004, ISSN: 0008-8846. DOI: 10.1016/j.cemconres.2004.05.034. [Online]. Available: https://www.sciencedirect.com/science/article/pii/S0008884604002364 (visited on 04/11/2022).

[5] ——, "The nature of C-S-H in hardened cements," en, *Cement and Concrete Research*, vol. 29, no. 8, pp. 1131–1147, Aug. 1999, ISSN: 0008-8846. DOI: 10.1016/S0008-8846(99)00168-4. [Online]. Available: https://www.sciencedirect.com/science/article/pii/S0008884699001684 (visited on 04/11/2022).

[6] A. Kumar, B. J. Walder, A. Kunhi Mohamed, *et al.*, "The Atomic-Level Structure of Cementitious Calcium Silicate Hydrate," en, *The Journal of Physical Chemistry C*, vol. 121, no. 32, pp. 17 188–17 196, Aug. 2017, ISSN: 1932-7447, 1932-7455. DOI: 10.1021/acs.jpcc.7b02439. [Online]. Available: https://pubs.acs.org/doi/10.1021/acs.jpcc.7b02439 (visited on 04/11/2022).

[7] A. Kunhi Mohamed, S. C. Parker, P. Bowen, and S. Galmarini, "An atomistic building block description of C-S-H - Towards a realistic C-S-H model," en, *Cement and Concrete Research*, vol. 107, pp. 221–235, May 2018, ISSN: 0008-8846. DOI: 10.1016/j.cemconres.2018.01.007. [Online]. Available: https://www.sciencedirect.com/science/article/pii/S0008884617302533 (visited on 04/11/2022).

[8] A. Morshedifard, S. Masoumi, and M. J. Abdolhosseini Qomi, "Nanoscale origins of creep in calcium silicate hydrates," en, *Nature Communications*, vol. 9, no. 1, p. 1785, May 2018, Number: 1 Publisher: Nature Publishing Group, ISSN: 2041-1723. DOI: 10.1038/s41467-018-04174-z. [Online]. Available: https://www.nature.com/articles/s41467-018-04174-z (visited on 04/11/2022).

[9] Z. Casar, A. K. Mohamed, M. Harris, P. Bowen, and K. Scrivener, "Calcium Silicate Hydrate Surfaces and How to Model Them (draft)," English, *Unpublished*, (visited on 02/18/2022).

[10] A. G. Kalinichev, J. Wang, and R. J. Kirkpatrick, "Molecular dynamics modeling of the structure, dynamics and energetics of mineral–water interfaces: Application to cement materials," en, *Cement and Concrete Research*, Cementitious Materials as model porous media: Nanostructure and Transport processes, vol. 37, no. 3, pp. 337–347, Mar. 2007, ISSN: 0008-8846. DOI: 10.1016/j.cemconres.2006.07.004. [Online]. Available: https://www.sciencedirect.com/science/article/pii/S0008884606001906 (visited on 04/11/2022).

[11] M. J. Abdolhosseini Qomi, L. Brochard, T. Honorio, I. Maruyama, and M. Vandamme, "Advances in atomistic modeling and understanding of drying shrinkage in cementitious materials," en, *Cement and Concrete Research*, vol. 148, p. 106 536, Oct. 2021, ISSN: 0008-8846. DOI: 10.1016/j.cemconres.2021.106536. [Online]. Available: https://www.sciencedirect.com/science/article/pii/S000888462100185X (visited on 04/11/2022).

[12] N. Marzari, "The frontiers and the challenges," en, *Nature Materials*, vol. 15, no. 4, pp. 381–382, Apr. 2016, ISSN: 1476-1122, 1476-4660. DOI: 10.1038/nmat4613. [Online]. Available: http://www.nature.com/articles/nmat4613 (visited on 04/13/2022).

[13] A. Kunhi Mohamed, S. A. Weckwerth, R. K. Mishra, H. Heinz, and R. J. Flatt, "Molecular modeling of chemical admixtures; opportunities and challenges," en, *Cement and Concrete Research*, vol. 156, p. 106 783, Jun. 2022, ISSN: 0008-8846. DOI: 10.1016/j.cemconres.2022.106783. [Online]. Available: https://www.sciencedirect.com/science/article/pii/S0008884622000746 (visited on 04/12/2022).

[14] J. Lopez, *Jlopez141/pyCSH*, original-date: 2021-10-14T07:23:45Z, Jan. 2022. [Online]. Available: https://github.com/jlopez141/pyCSH (visited on 06/09/2022).

[15] A. P. Thompson, H. M. Aktulga, R. Berger, *et al.*, "LAMMPS - a flexible simulation tool for particle-based materials modeling at the atomic, meso, and continuum scales," en, *Computer Physics Communications*, vol. 271, p. 108 171, Feb. 2022, ISSN: 0010-4655. DOI: 10.1016/j.cpc.2021.108171. [Online]. Available: https://www.sciencedirect.com/science/article/pii/S0010465521002836 (visited on 06/08/2022).

[16] M. Valavi, Z. Casar, A. Kunhi Mohamed, P. Bowen, and S. Galmarini, "Molecular dynamic simulations of cementitious systems using a newly developed force field suite ERICA FF," en, *Cement and Concrete Research*, vol. 154, p. 106 712, Apr. 2022, ISSN: 0008-8846. DOI: 10.1016/j.cemconres.2022.106712. [Online]. Available: https://www.sciencedirect.com/science/article/pii/S0008884622000035 (visited on 06/09/2022).

[17] *General · jfbonvin/CSH_interlayer*, en. [Online]. Available: https://github.com/jfbonvin/CSH_interlayer (visited on 06/15/2022).

[18] Ali, *Answer to "Check which side of a plane points are on"*, Mar. 2013. [Online]. Available: https://stackoverflow.com/a/15691064/16000924 (visited on 06/11/2022).

[19] J. D. Hunter, "Matplotlib: A 2D graphics environment," *Computing in Science & Engineering*, vol. 9, no. 3, pp. 90–95, 2007, Publisher: IEEE COMPUTER SOC. DOI: 10.1109/MCSE.2007.55.

[20] *Kernel density estimation*, en, Page Version ID: 1090270394, May 2022. [Online]. Available: https://en.wikipedia.org/w/index.php?title=Kernel_density_estimation&oldid=1090270394 (visited on 06/08/2022).

[21] *How to draw a contour plot in matplotlib*. [Online]. Available: https://www.educative.io/answers/how-to-draw-a-contour-plot-in-matplotlib (visited on 06/14/2022).

[22] M. Gimond, *Chapter 11 Point Pattern Analysis — Intro to GIS and Spatial Analysis*. [Online]. Available: https://mgimond.github.io/Spatial/chp11_0.html (visited on 06/08/2022).

[23] H. Weltens, H. Bressler, F. Terres, H. Neumaier, and D. Rammoser, "Optimisation of Catalytic Converter Gas Flow Distribution by CFD Prediction," English, SAE International, Warrendale, PA, SAE Technical Paper 930780, Mar. 1993, ISSN: 0148-7191, 2688-3627. DOI: 10.4271/930780. [Online]. Available: https://www.sae.org/publications/technical-papers/content/930780/ (visited on 05/03/2022).

[24] L. Pauling, "THE PRINCIPLES DETERMINING THE STRUCTURE OF COMPLEX IONIC CRYSTALS," *Journal of the American Chemical Society*, vol. 51, no. 4, pp. 1010–1026, Apr. 1929, Publisher: American Chemical Society, ISSN: 0002-7863. DOI: 10.1021/ja01379a006. [Online]. Available: https://doi.org/10.1021/ja01379a006 (visited on 06/10/2022).